Journal of Organometallic Chemistry xxx (2015) 1–10

Contents lists available at ScienceDirect

Journal of Organometallic Chemistry

journal homepage: www.elsevier.com/locate/jorganchem

The [*closo*-$B_{12}H_{11}$-1-IAr]$^-$ zwitterion as a precursor to monosubstituted derivatives of [*closo*-$B_{12}H_{12}$]$^{2-}$

Paweł Tokarz [a], Piotr Kaszyński [a, b, c, *], Sławomir Domagała [d], Krzysztof Woźniak [d]

[a] Organic Materials Research Group, Department of Chemistry, Middle Tennessee State University, TN, 37123, USA
[b] Faculty of Chemistry, University of Łódź, 91403, Łódź, Poland
[c] Centre of Molecular and Macromolecular Studies, Polish Academy of Sciences, 90363, Łódź, Poland
[d] Department of Chemistry, University of Warsaw, 02-089, Warsaw, Poland

ARTICLE INFO

Article history:
Received 28 April 2015
Received in revised form
20 July 2015
Accepted 21 July 2015
Available online xxx
Dedicated to Professor Russell Grimes on the occasion of 80th birthday.

Keywords:
Closo-borates
Iodonium zwitterions
B–H activation
Functionalization
DFT calculation
Mechanism

ABSTRACT

Reactions of [*closo*-$B_{12}H_{12}$]$^{2-}$ with ArI(OAc)$_2$ in aqueous AcOH in the presence of [NEt_4]$^+$ or [$NHEt_3$]$^+$ give [*closo*-$B_{12}H_{11}$-1-IAr]$^-$ (**1**) in 74–95% yield as a white precipitate. The zwitterions decompose in CD_3CN solutions with rates $k = 3.30 \pm 0.04 \times 10^{-4}$ s^{-1} (Ar = Ph, **1a[NEt$_4$]**) and $k = 1.96 \pm 0.01 \times 10^{-4}$ s^{-1} (Ar = C_6H_4OMe-4, **1b[NEt$_4$]**) at 0 °C. Reactions of the zwitterion with Me_2NCHS and pyridine gave the corresponding products [*closo*-$B_{12}H_{11}$-1-SCHNMe$_2$]$^-$ (**2**) and [*closo*-$B_{12}H_{11}$-1-NC_5H_5]$^-$ (**3**) isolated in 25–27% and up to 44% yield, respectively. The former anion is a protected thiol derivative, which was transformed to the sulfonium derivative [*closo*-$B_{12}H_{11}$-1-S(CH$_2$)$_5$]$^-$ (**8**). The molecular structure and spectroscopic properties of pyridinium zwitterion **3** were analyzed experimentally and computationally (B3LYP), and results compared with those for the [*closo*-$B_{10}H_9$-1-NC_5H_5]$^-$ (**4**) analog. Mechanisms of formation of **2**–**4** from appropriate aryliodonium zwitterions were analyzed with the M062x computational method.

1. Introduction

A half a century of systematic investigation of the [*closo*-$B_{12}H_{12}$]$^{2-}$ anion (**A**, Fig. 1) has resulted in the development of a plethora of functionalization methods and discovery of a wealth of functional derivatives [1]. These investigations intensified about 25 years ago with the onset of the boron neutron capture therapy (BNCT) technology [2]. Consequently many methods leading to mono-functionalized derivatives of [*closo*-$B_{12}H_{12}$]$^{2-}$ have been refined and a number of compounds have been tested for suitability in medicinal applications [3,4]. The target compounds are typically prepared using a handful of key intermediates (Fig. 1) taking advantage of straightforward transformations of a single simple functional group [5]. Thus, carbonyl derivative **B** [6], isocyanate **C** [7] and oxonium zwitterions **D** and **E** [8] are reacted with nucleophiles; iodide **F** [9,10] has been demonstrated to undergo B–C coupling with organometallic reagents in the presence of a Pd catalyst [11,12], while derivatives **G** [13], **H** [14] and **I** [15] undergo facile reactions with a range of electrophiles. These synthetic handles allowing for incorporation of the [*closo*-$B_{12}H_{12}$]$^{2-}$ cluster to more complex molecular architectures are introduced by direct activation of the B–H bonds under acidic conditions, often involving Brønsted acid catalysis and elevated temperatures [1]. Methods for preparing these intermediates and their transformations have been reviewed extensively [1,4,8].

Recently we have discovered another method for activation of the B–H bonds in *closo*-borates towards substitution by converting them into aryliodonium zwitterions, and demonstrated their reactions with a number of nucleophiles [16]. We have demonstrated this method also for the parent anion [*closo*-$B_{12}H_{12}$]$^{2-}$ (**A**) and its dimethylsulfonium derivative [*closo*-$B_{12}H_{11}$-1-SMe_2]$^-$, and isolated relatively stable and synthetically useful bis-zwitterions (Fig. 2). Surprisingly, mono-aryliodonium derivatives of the [*closo*-$B_{12}H_{12}$]$^{2-}$, that could lead to mono-functionalized derivatives, were not observed in these reactions.

Here we report the preparation of two mono-aryliodonium zwitterions [*closo*-$B_{12}H_{11}$-1-IAr]$^-$ (**1**) and investigate their

* Corresponding author. Organic Materials Research Group, Department of Chemistry, Vanderbilt University, Box 1822 Station B, Nashville, TN, 37235, USA.
E-mail address: piotr.kaszynski@vanderbilt.edu (P. Kaszyński).

http://dx.doi.org/10.1016/j.jorganchem.2015.07.035
0022-328X/

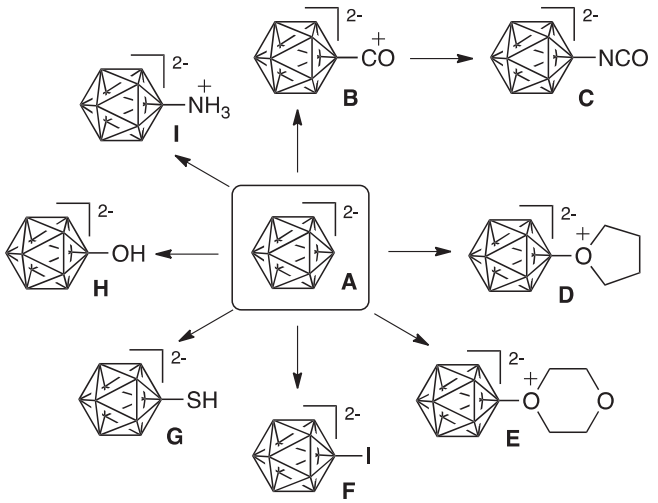

Fig. 1. Mono-functional synthetic intermediates **B**–**I** derived from the [*closo*-$B_{12}H_{12}$]$^{2-}$ anion (**A**). Each unsubstituted vertex represents a BH fragment.

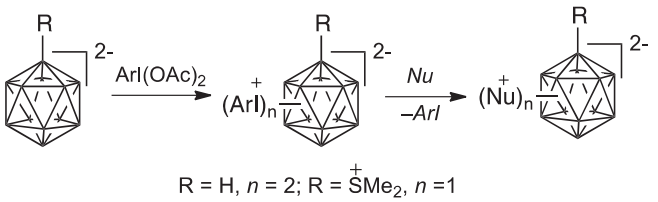

Fig. 2. B–H activation in [*closo*-$B_{12}H_{12}$]$^{-2}$ through aryliodoniation. Ref. [16].

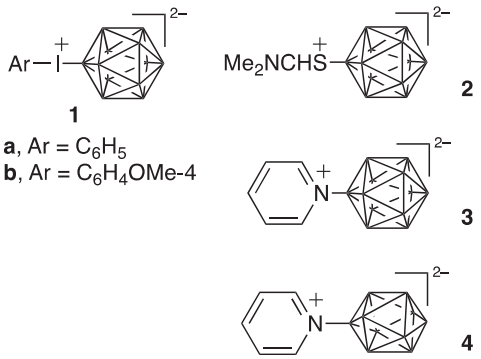

Fig. 3. The structures of zwitterions **1**–**4**.

application for the synthesis of protected mercaptan **2** and pyridinium zwitterion **3** (Fig. 3). The usefulness of **2** as a synthetic intermediate is demonstrated by alkylative cyclization, while pyridinium **3** is compared to its 10-vertex analog **4** by spectroscopic and XRD methods augmented with DFT calculations. Finally, mechanisms for the formation of **2**–**4** were investigated with the DFT methods.

2. Results

2.1. Synthesis

Initial attempts at preparation of mono-aryliodonium zwitterions [*closo*-$B_{12}H_{11}$-1-IAr]$^{-}$ [NEt_4]$^{+}$ (**1[NEt$_4$]**) following a general method [16] were unsuccessful. The expected product could not be isolated, while analysis of the reaction mixtures revealed complete reduction of ArI(OAc)$_2$, as evident from the presence of iodobenzene and 4-iodoanisole as the only organic products. Suspecting low thermal stability of zwitterion **1** in solutions, the solvent system was adjusted in such a way that the product was insoluble and could be isolated by filtration. Through systematic experimentations, the reaction conditions were optimized and crude phenyliodonium (**1a[NEt$_4$]**) and 4-methoxyphenyliodonium (**1b[NEt$_4$]** and **1b[NHEt$_3$]**) derivatives were isolated in 74–95% yield. Thus, a solution of **A[2Na]** in AcOH was added to a solution of ArI(OAc)$_2$ and [NEt_4]$^{+}$AcO^{-} or [$NHEt_3$]$^{+}$AcO^{-} in 70% aqueous AcOH at 0 °C, and after 30 min the product was filtered (Scheme 1). The reaction appears to be rapid giving essentially pure product, as assessed by low temperature ^{1}H NMR.

Time-depended ^{1}H NMR studies of CD_3CN solutions of mono-aryliodonium derivatives **1** indeed revealed their relatively fast decomposition even at low temperature with rates $k = 3.30 \pm 0.04 \times 10^{-4}$ s^{-1} for **1a[NEt$_4$]** and $k = 1.96 \pm 0.01 \times 10^{-4}$ s^{-1} for **1b[NEt$_4$]** at 0 °C. Analysis of the ^{1}H NMR spectra demonstrated that in the case of **1a[NEt$_4$]** the main organic product was iodobenzene, while decomposition of 4-methoxyphenyliodonium analog **1b[NEt$_4$]** resulted in two sets of doublets, with the more downfield one identified as 4-iodoanisole (Fig. 4). At higher temperatures (e.g. 25 °C) 4-iodoanisole is the main organic product. MS analysis of the solutions suggests that the main decomposition products of **1** containing boron are {*closo*-B_{12}} cage arylated product, such as **5**, and nitrilium ylide **6**, which hydrolyzes to acetamide derivative **7** (Scheme 2).

In spite of low thermal stability, aryliodonium zwitterions **1[NEt$_4$]** appear to be useful intermediates to other monosubstituted derivatives of [*closo*-$B_{12}H_{12}$]$^{2-}$. In general, the 4-methoxyphenyliodonium derivative **1b[NEt$_4$]** gives higher yields of the substitution products than the phenyliodonium analog **1a[NEt$_4$]** under the same conditions. Also, higher yields are obtained at lower temperatures. Thus, a reaction of **1b[NEt$_4$]** with Me_2NCHS gave the protected mercaptan **2[NEt$_4$]** (Scheme 1) in 25–27% yield at −10 °C. Synthetic utility of **2[NEt$_4$]** was subsequently demonstrated by alkylative cyclization with pentamethylene dibromide under basic hydrolytic conditions and the formation of sulfonium derivative **8[NEt$_4$]** in 82% yield (Scheme 3).

A similar reaction of **1b[NEt$_4$]** with pyridine at −10 °C led to the formation of pyridinium derivative **3[NEt$_4$]** (Scheme 1) isolated in yields up to 44%. The same reaction of **1b[NHEt$_3$]** resulted in **3[NHEt$_3$]** obtained in 41% yield, while the phenyl analog **1a[NEt$_4$]**

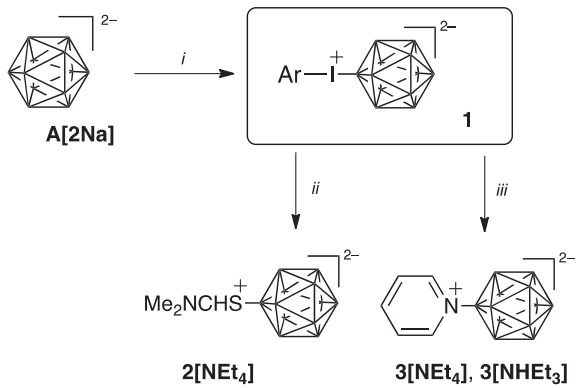

Scheme 1. Synthesis of zwitterinic derivatives **1**–**3**. Reagents and conditions: *i*) H_2O, PhI(OAc)$_2$ or 4-MeOC$_6$H$_4$I(OAc)$_2$, [NEt_4]$^{+}$AcO^{-} or [$NHEt_3$]$^{+}$AcO^{-} in 70% AcOH, 0 °C, 30 min; *ii*) Me_2NCHS, −10 °C, overnight; *iii*) Pyridine −10 °C, overnight.

Please cite this article in press as: P. Tokarz, et al., Journal of Organometallic Chemistry (2015), http://dx.doi.org/10.1016/j.jorganchem.2015.07.035

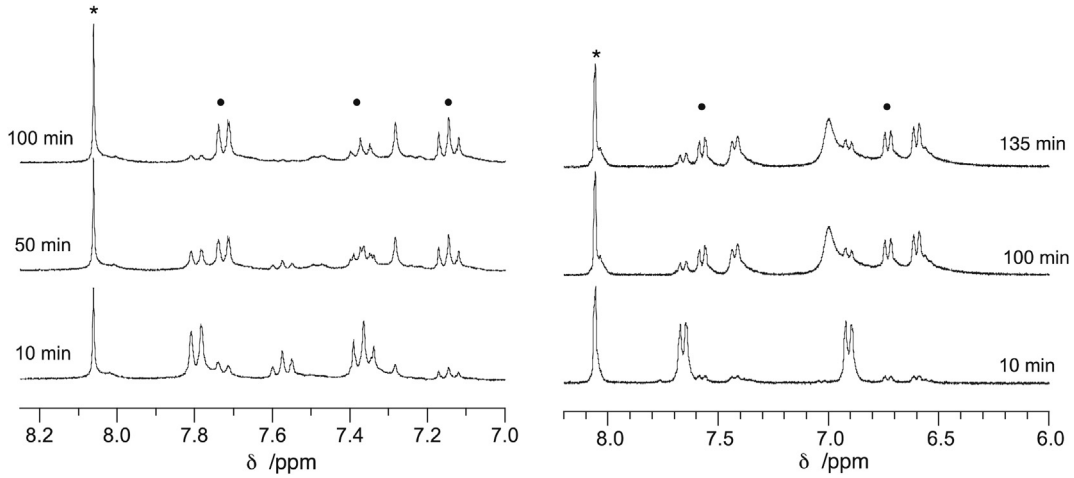

Fig. 4. ^{1}H NMR spectra of [*closo*-$B_{12}H_{11}$-1-IPh]$^-$[NEt_4]$^+$ (**1a[NEt$_4$]**, left) and [*closo*-$B_{12}H_{11}$-1-(IC_6H_4OMe-4)]$^-$[NEt_4]$^+$ (**1b[NEt$_4$]**, right) recorded in CD_3CN at 0 °C. The asterisk marks the signal of dimethyl terephthalate reference and the dots the appropriate iodoarene.

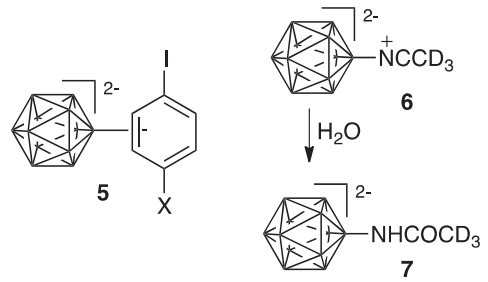

Scheme 2. Proposed boron-containing products of thermolysis of **1** in CD_3CN.

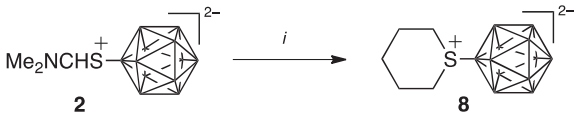

Scheme 3. Synthesis of sulfonium zwitterion **8**. Reagents and conditions: *i*) $Br(CH_2)_5Br$, MeCN, [NEt_4]$^+OH^-$, reflux, overnight.

gave product **3[NEt$_4$]** in significantly lower yields (12%). In all these reactions, the major by-product was identified as cage arylation product(s), presumably **5**.

2.2. Comparative analysis of pyridinium derivatives **3** and **4**

Analysis of electronic and molecular structures of the pyridinium derivative **3** and comparison with those for the 10-vertex analog **4** provide an opportunity to gain a better understanding of electronic interactions between π-aromatic substituents, such as the pyridinium fragment, and σ-aromatic [17] *closo*-borates. Therefore, derivatives [*closo*-$B_{12}H_{11}$-1-NC_5H_5]$^-$ (**3**) and [*closo*-$B_{10}H_9$-1-NC_5H_5]$^-$ (**4**) [16] were investigated in detail by computational, spectroscopic, and XRD methods.

2.2.1. Electronic structures

NBO population analysis of the B3LYP/6-31G(2d,p) wavefunctions demonstrates some differences in electron density distribution in derivatives **3** and **4**, as shown in Table 1. In both compounds the B(1)–N bond has a dative character. The substituted B(1) atom has higher positive charge in the 12-vertex derivative than in **4**, which demonstrates greater electron withdrawing ability of the former. Consequently, more electron density is depleted from the carbon atoms in positions 2, 4, and 6 of the pyridine ring in **3** (Table 1) relative to the 10-vertex analog **4**.

Table 1
Selected electronic parameters for **3** and **4**.

	3	**4**
$q_{B(1)}$[a]	+0.095	−0.012
q_N[a]	−0.393	−0.394
$q_{C(2,6)}$[a]	+0.089	+0.060
$q_{C(3,5)}$[a]	−0.270	−0.270
$q_{C(4)}$[a]	−0.198	−0.230
δ ($H_{2,6}$)/ppm[b]	9.01	9.49[c]
δ ($H_{3,5}$)/ppm[b]	7.65	7.77[c]
δ (H_4)/ppm[b]	8.16	8.25[c]
δ (C_4)/ppm[b]	143.3	142.2[c]

[a] Atomic charge from the NBO analysis of the B3LYP/6-31G(2d,p) wavefunction.
[b] NMR chemical shift of the pyridine fragment in CD_3CN.
[c] Ref. [16].

The difference in electron distribution and their dynamics in the two compounds affect the chemical shifts in NMR spectroscopy: the "organic" H atoms are generally more shielded and carbon atoms are deshielded in **3** relative to those in **4**. For instance, hydrogen atoms in positions 2/6 of the pyridine ring are shielded by 0.48 ppm and the C(4) carbon atom is deshielded by 1.1 ppm in the 12-vertex derivative **3** relative to the 10-vertex analog **4** (Table 1).

2.2.2. Electronic absorption spectroscopy

Both compounds **3[NEt$_4$]** and **4[NEt$_4$]** exhibit a single major absorption band in the UV region above 200 nm with maxima at 266.5 nm ($\log \varepsilon = 3.87$) and 364.5 nm ($\log \varepsilon = 3.85$), respectively in MeCN (Fig. 5). In addition, 10-vertex derivative **4[NEt$_4$]** exhibits a lower intensity band at 244.5 nm, while the 12-vertex analog **3** has shoulder absorption at about 220 nm. Interestingly, the main absorption band in **3** exhibits a vibronic structure with separation of about 100 meV.

TD–DFT computational analysis (TD-B3LYP/6-31G(2d,p)) of both anions in MeCN dielectric medium reproduced well the experimental spectra. The lowest energy electronic excitation in **3** is calculated at 293.5 nm ($f = 0.161$) and involves a transition

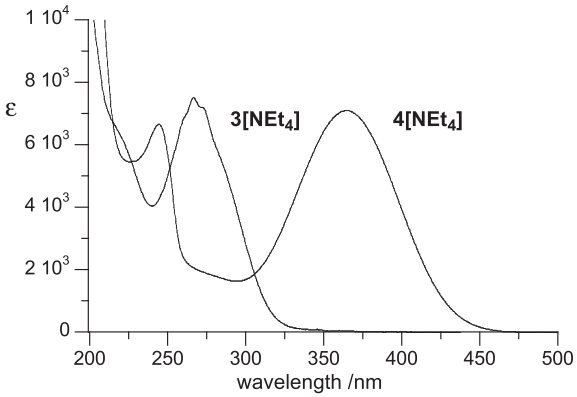

Fig. 5. Electronic absorption spectra for **3[NEt$_4$]** and **4[NEt$_4$]** (CH_3CN).

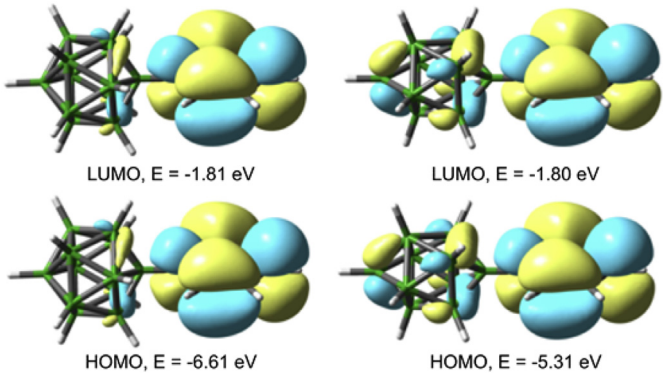

Fig. 6. TD-B3LYP/6-31G(2d,p) – derived contours and energies of molecular orbitals relevant to low energy excitations in **3** (left) and **4** (right) in CD_3CN.

mainly from the HOMO, localized on the cluster, to the LUMO, localized on the pyridine fragment (Fig. 6). Higher energy transitions involving the cage-to-ring excitation are of lower intensity ($f \approx 0.02$) and occur at 291.5 nm, 261 nm, and 241 nm. Similar TD–DFT analysis for the 10-vertex analog **4**, demonstrated a significantly lower energy HOMO → LUMO excitation at 406 nm ($f = 0.284$), and minor low intensity cage-to-ring excitations at 278 nm ($f = 0.06$) and 246 nm ($f = 0.03$) [18]. These excitations energies are consistent with the relative energies of the FMOs: while the LUMO is calculated at similar energy of about −1.8 eV for both derivatives, the HOMO of the 12-vertex derivative **3** is 1.3 eV lower than that of the 10-vertex analog. This difference corresponds to the experimentally observed 1.25 eV difference in excitation energy of the two compounds, as demonstrated in Fig. 5.

2.2.3. X-ray crystallography

Colorless crystals of **3[NEt$_4$]**, **3[NHEt$_3$]**, and yellow crystals of **4[NEt$_4$]** were obtained from MeOH and aqueous EtOH, respectively, and their solid-state structures were determined by low temperature single crystal X-ray analysis. Results are shown in Tables 2 and 3 and in Fig. 7.

The [*closo*-$B_{12}H_{11}$-1-NC_5H_5]$^-$ [NEt_4]$^+$ (**3[NEt$_4$]**) ion pair crystallizes in a *R*3*c* trigonal space group with a unit cell containing eighteen molecules, while the [$NHEt_3$] analog, **3[NHEt$_3$]**, gives crystals with a $P2_1/n$ monoclinic space group and four molecules in the unit cell. Analysis of crystals of the 10-vertex analog [*closo*-$B_{10}H_9$-1-NC_5H_5]$^-$ [NEt_4]$^+$ (**4[NEt$_4$]**) revealed a $P2_1$ monoclinic space group with a unit cell containing two pairs of unique molecules. One of them is superimposed in a 5:1 ratio with the 6-chloro analog

Table 2
Crystallographic data for **3[NEt$_4$]**, **3[NHEt$_3$]**, and **4[NEt$_4$]**.[a]

	3[NEt$_4$]	3[NHEt$_3$]	4[NEt$_4$]
Empirical formula	$C_{13}H_{36}B_{12}N_2$	$C_{11}H_{32}B_{12}N_2$	$C_{13}H_{33.9}B_{10}Cl_{0.1}N_2$
fw	350.16	322.10	330.05
Space group	*R*3*c*	$P2_1/n$	$P2_1$
a, Å	27.798(1)	8.1295(1)	11.8538(2)
b, Å	27.798(1)	14.1665(2)	11.5995(2)
c, Å	14.7840(5)	17.1661(2)	15.8114(3)
α, deg	90	90	90
β, deg	90	90.009(1)	107.348(2)
γ, deg	120	90	90
V, Å^3	9893.3(6)	1952.56(5)	2075.14(6)
Z	18	4	4
ρ (calcd), g/cm^3	1.058	1.096	1.056
μ, mm^{-1}	0.053	0.054	0.066
R_{int}	0.0644	0.0272	0.0259
R[b] (I > 2σ(I))	0.0456	0.0497	0.0446
R_w[c] (I > 2σ(I))	0.0970	0.1382	0.1229
R (all data)	0.0617	0.0568	0.0500
R_w (all data)	0.1041	0.1439	0.1275
Goodness of fit on F^2	1.031	1.072	1.067

[a] Temperature 100 K, λ = 0.71073 Å.
[b] $R = \sum||Fo| - |Fc||/\sum|Fo|$.
[c] $R_w = [\sum[w(Fo^2 - Fc^2)^2]/\sum[w(Fo^2)^2]]^{1/2}$.

Table 3
Selected interatomic distances and angles for **3[NHEt$_3$]**, **3[NEt$_4$]** and **4[NEt$_4$]**.

	3[NEt$_4$]	3[NHEt$_3$]	4[NEt$_4$][a]
N–B	1.559(3)	1.564(1)	1.530(3)
B(1)–B(2)[b]	1.768(2)	1.773(5)	1.677(4)
B(2)–B(3)[b]	1.794(7)	1.789(3)	1.847(4)
B(2)–B(6/7)[b]	1.782(3)	1.780(5)	1.809(6)
B(6/7)–B(7/8)[b]	1.786(5)	1.785(7)	1.838(7)
B(6/7)–B(10/12)[b]	1.781(5)	1.784(4)	1.700(6)
B–B(1)–N[b]	120.4(6)	120(1)	128.9(4)
B–B(10/12)–H[b]	121.5(2)	121.7(2)	130.1(2)
B(1) ⋯ B(10/12)	3.338(4)	3.358(2)	3.657(4)

[a] Unperturbed molecule.
[b] Average values.

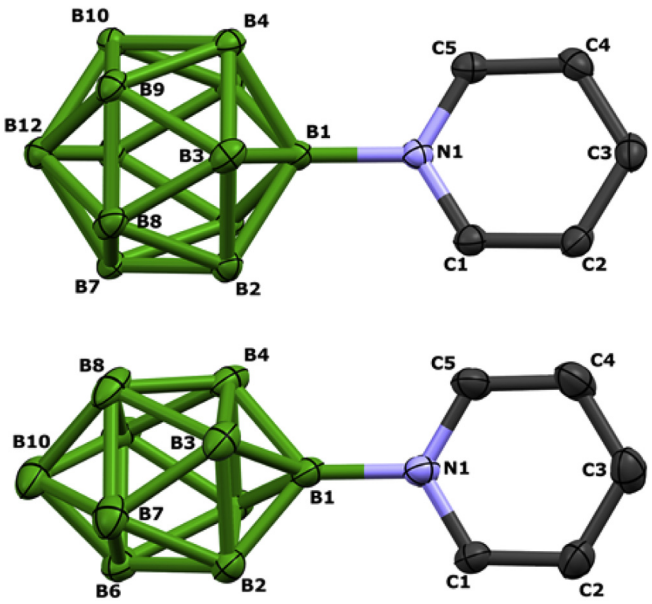

Fig. 7. Thermal ellipsoid diagram drawn at 50% probability for 1-pyridinium-dodecaborate (**3[NEt$_4$]**, top) and 1-pyridinium-decaborate (**4[NEt$_4$]**, bottom). Hydrogen atoms and the cations are omitted for clarity. Pertinent molecular dimensions are listed in Table 3.

[*closo*-$B_{10}H_8$-6-Cl-1-NC_5H_5]$^-$ [NEt_4]$^+$, an impurity that apparently originates from the phenyliodoniation of the parent cluster [*closo*-$B_{10}H_{10}$]$^{2-}$. Therefore, analysis of the molecular structure was limited to the unperturbed molecule.

Molecular geometry analysis revealed that the B(1)–N bond in **3[NEt$_4$]** (1.559(3) Å, Table 3) is longer by about 3 pm than that in the 10-vertex analog **4[NEt$_4$]** (1.530(3) Å), which is in good agreement with computational results (1.556 Å and 1.499 Å, respectively at the B3LYP/6-31G(2d,p) level of theory). The biggest difference between the experimental and theoretical structures is the orientation of the pyridine ring relative to the cage. While the gas phase structures of the anions prefer the staggered conformation, experimental results demonstrate essentially eclipsed, in **3[NEt$_4$]** (1.7(3)°), and partially eclipsed, in **3[NHEt$_3$]** (9.7(2)°) and **4[NEt$_4$]** (20.2(3)°), orientation of the pyridine ring.

Further analysis demonstrated that substitution of the pyridine ring on the cluster distorts bonding of the boron atom to its neighbors. Thus, in both derivatives the B(1)–B bonds and the N–B(1)–B angles are slightly contracted relative to those of the unsubstituted antipodal B vertex in response diminished electron density (Table 3). These experimental results are consistent with those obtained with the DFT methods.

2.3. Mechanistic considerations

Substitution of the pyridine fragment onto the [*closo*-$B_{12}H_{12}$]$^{2-}$ cluster in **3** is a two-step process: introduction of the aryliodonium, a labile leaving group, and formation of the pyridine-B(1) bond either through an addition-elimination mechanism (involving the 10-I-3 intermediate) [16] or through elimination-addition mechanism (S_N1–type process). A competing process is arylation of the {*closo*-B_{12}} cluster. All three processes, shown in Fig. 8, were investigated in detail at the M062x/6-31+G(2d,p)//M062x/6-31G(2d,p) level of theory in dielectric media of an appropriate solvent. Results for the transformation of iodonium **1** to pyridinium **3** were compared to those of the analogous transformation of [*closo*-$B_{10}H_9$-1-IPh]$^-$ (**9**) to **4** shown in Fig. 9, and expanded to analysis of the formation of **2** from **1** (Fig. 10). Selected relevant structures with DFT-optimized geometries are shown in Figs. 11 and 12.

Computational analysis demonstrate that **1a** (Ar = Ph) forms a weak adduct with pyridine, **1a-Pyr**, in which the pyridine ring is perpendicular to the {*closo*-B_{12}} cage and N ⋯ I distance (3.011 Å) is 0.52 Å inside the van der Waals separation in the global minimum (Fig. 8). The analogous local minimum is 1.50 kcal mol^{-1} higher in energy, in which the N ⋯ I distance is longer (3.305 Å), and the pyridine ring is approximately parallel to the {*closo*-B_{12}} cage appropriate for the TS geometry (Fig. 11). The transition state, **1a/3–TS**, to the formation of substitution product **3** is $\Delta G^{\ddagger}_{298}$ = 15.50 kcal mol^{-1} above the local minimum in pyridine dielectric medium (Fig. 8). Elimination of PhI from the TS structure **1a/3–TS** and formation of **3** is highly exothermic (ΔH = −60.5 kcal mol^{-1}), as was found for reaction of other such boronium ylides [19,20].

In an alternative mechanism the B–I bond in **1a** (Ar = Ph) undergoes heterolysis through a transition structure **1a-TS** in which the B(1) migrates from the iodine atom to the iodone–C(1) bond (Figs. 8 and 11). The calculated free energy of activation is $\Delta G^{\ddagger}_{298}$ = 15.45 kcal mol^{-1} in pyridine dielectric medium, which is essentially the same as for the formation of **1a/3-TS** making these two processes nearly equally probable. The transition structure **1a-TS** may undergo entropically driven fragmentation giving rise to the reactive boronium ylide **10**, which reacts with pyridine giving **3**. Stabilization of structure **1a-TS** may also involve shifting of the boron atom from the iodine-C(1) bond in **1a-TS** to the C(2) position in intermediate **11a** (Fig. 11), which is consistent with electrophilic attack of the ylide **10** on the benzene ring. The intermediate **11a** is presumably stabilized by deprotonation and formation of a byproduct of type **5**. The latter of the two pathways is exothermic although less exergonic by 2.5 kcal mol^{-1} relative to the formation of ylide **10**, thus less preferred kinetically.

The two processes, rearrangement of the zwitterion **1a** and its complex with pyridine **1a-Pyr**, have essentially the same calculated free energy of activation at ambient temperature, $\Delta G^{\ddagger}_{298}$. They have, however, different entropy of activation and hence their rates exhibit different temperature dependence. Thus, $\Delta S^{\ddagger}$ for rearrangement of **1a** is +4.3 cal mol^{-1} K^{-1}, while for **1a-Pyr** is only +0.7 cal mol^{-1} K^{-1}. Consequently, lowering the temperature will increase $\Delta G^{\ddagger}$ more for the former making the latter process more efficient. This is consistent with experimental observations: lowering the temperature increases the yield of product **3**.

Substitution of the methoxy group into the benzene ring in **1a** modestly stabilizes the zwitterion **1b** against decomposition, as evident in Fig. 8 and in agreement with experiment. Thus, the

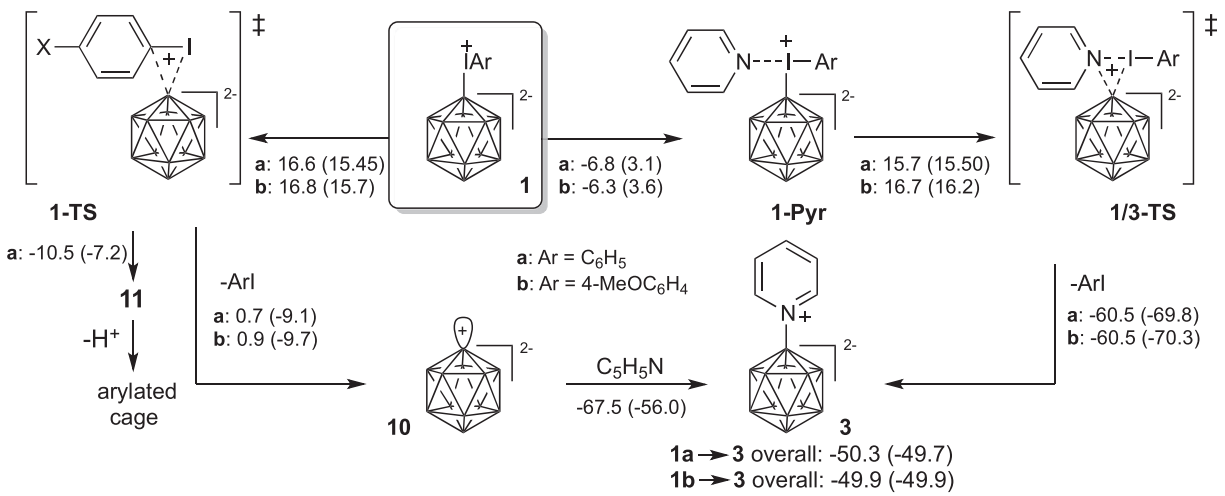

Fig. 8. Two mechanisms for the formation of **3**. Enthalpy, ΔH, and free energy change at 298 K, ΔG_{298} (in parentheses), for each step were calculated using the M062x/6-31+G(2d,p)//M062x/6-31G(2d,p) method in pyridine dielectric medium (the PCM model) and are in kcal/mol. Equilibrium geometry of selected structures are shown in Fig. 11.

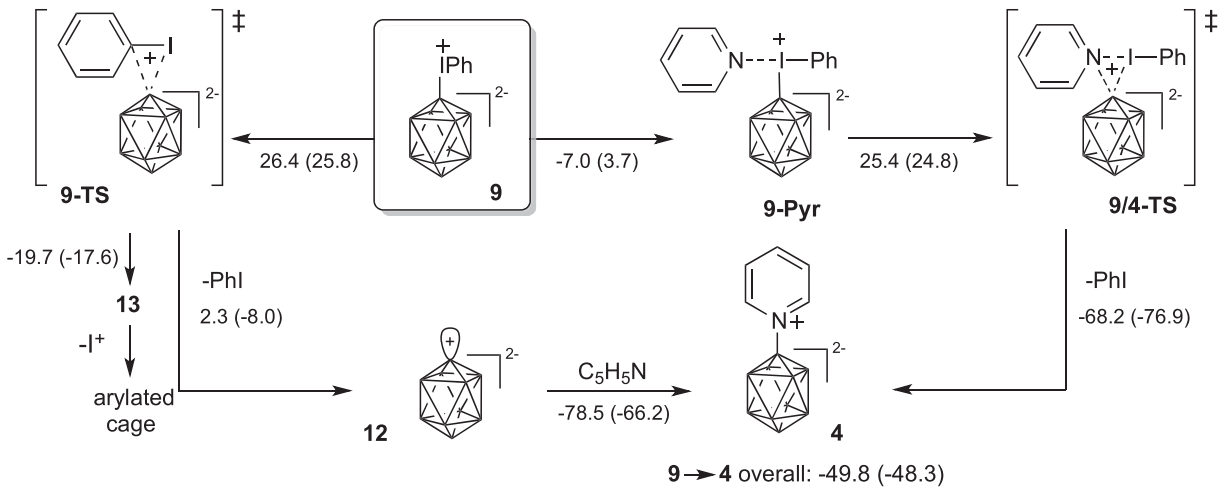

Fig. 9. Two mechanisms for the formation of **4**. Enthalpy, ΔH, and free energy change at 298 K, ΔG_{298} (in parentheses), for each step were calculated using the M062x/6-31+G(2d,p)//M062x/6-31G(2d,p) method in pyridine dielectric medium (the PCM model) and are in kcal/mol. Equilibrium geometry of selected structures are shown in Fig. 12.

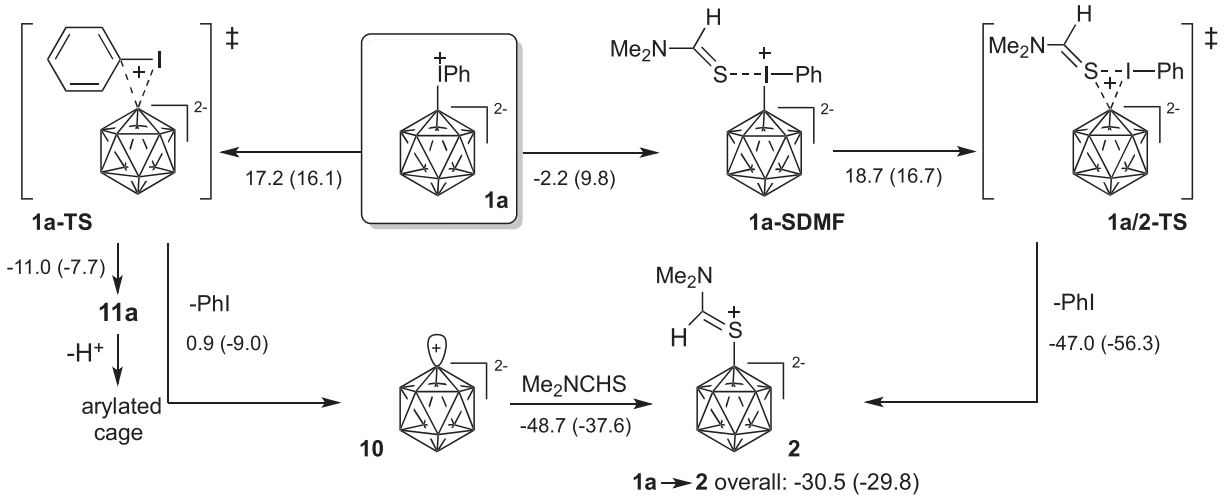

Fig. 10. Two mechanisms for the formation of **2**. Enthalpy, ΔH, and free energy (in parentheses) change at 298 K, ΔG_{298}, for each step were calculated using the M062x/6-31+G(2d,p)//M062x/6-31G(2d,p) method in Me_2NCHS dielectric medium (the PCM model) and are given in kcal/mol. Equilibrium geometry of selected structures are shown in Fig. 11.

electron-donating MeO group destabilizes the complex with pyridine **1b-Pyr** by 0.5 kcal mol^{-1} (weaker electrostatic interaction between I and N) and increases free energy of activation by 0.7 kcal mol^{-1}. The rates of transformations of the methoxy analogs **1b** and **1b-Pyr** exhibit similar sensitivity to temperature due to differences in entropy of activation, and lower temperature favors the formation of **3**. Interestingly, in the intermediate **11b**, formed from **1b-TS**, the boronium atom B(1) interacts with the C(1) atom of in 4-iodoanisole, which has the highest electron density.

Similar analysis of the 10-vertex analog [*closo*-$B_{10}H_9$-1-IPh]$^-$ (**9**) revealed significantly different reactivity when compared to **1a**: the activation energies for rearrangements of **9** and **9-Pyr** are higher by about 10 kcal mol^{-1} than those in **1a** analogs, and the rearrangement of **9-Pyr** to pyridinium **4** is more favorable by 1.0 kcal mol^{-1} than rearrangement of **9** through **9-TS** (Figs. 9 and 12). Also, the formation of the boronium ylide **12** from **9-TS** is completely disfavored and formation of the intermediate **13** is the main stabilization pathway. These computational results are consistent with experimental observations [16]: in contrast to **1a**, reactions of **9** with pyridine require higher temperatures and pyridinium zwitterion **4** is the sole product. The overall enthalpy change in transforming of [*closo*-$B_{10}H_9$-1-IPh]$^-$ (**9**) to pyridinium **4** is −49.8 kcal mol^{-1} (or ΔG_{298} = −48.3 kcal mol^{-1}), which is nearly the same as for the 12-vertex analogs. Interestingly, in contrast to rearrangement of **1a**, the structure of the intermediate **13** is consistent with the electrophilic attack of boronium ylide **12** on the *ipso* C(1) position in PhI (Fig. 12), and thus its stabilization may involve deiodination and formation of [*closo*-$B_{10}H_9$-1-Ph]$^{2-}$.

The significant difference in the stability of zwitterions **1a** and **9** correlates with the calculated B–I distance: long, ~2.28 Å, in **1a** and **1b** derivatives and shorter, 2.169 Å, in analog **9** (Figs. 11 and 12). At the same time, the C–I distances are shorter in **1** (2.102 Å for Ph and 2.100 Å for 4-$MeOC_6H_4$) than in **9** (2.115 Å), which again is consistent with less B–I bonding in the former when compared to **9**. The interatomic distances in [*closo*-$B_{10}H_9$-1-IPh]$^-$ (**9**) are in a good agreement with experimental values of d_{B-I} = 2.194(13) Å and d_{C-I} = 2.159(12) Å [21].

Finally, we assessed the thermodynamics and kinetics of the formation of the sulfonium zwitterion **2** from iodonium **1a** (Fig. 10). Results of DFT calculations revealed that the free energy of

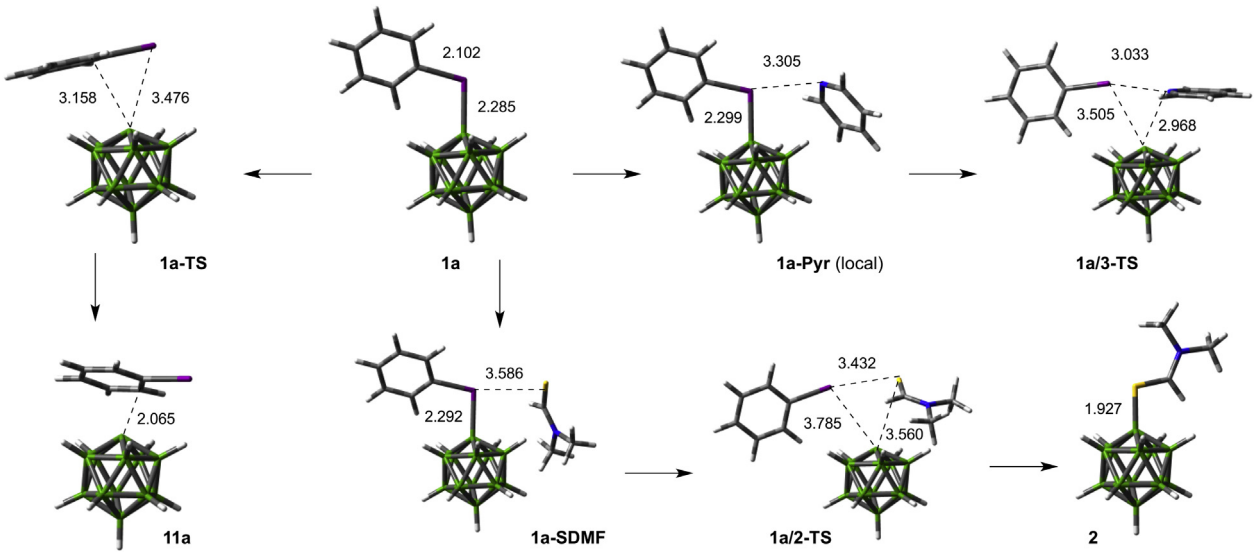

Fig. 11. Equilibrium geometry of species involved in transformations of [*closo*-$B_{12}H_{11}$-1-IPh]$^-$ (**1a**, C_1 molecular symmetry) at the M062x/6-31G(2d,p) level of theory. Selected interatomic distances are in Å.

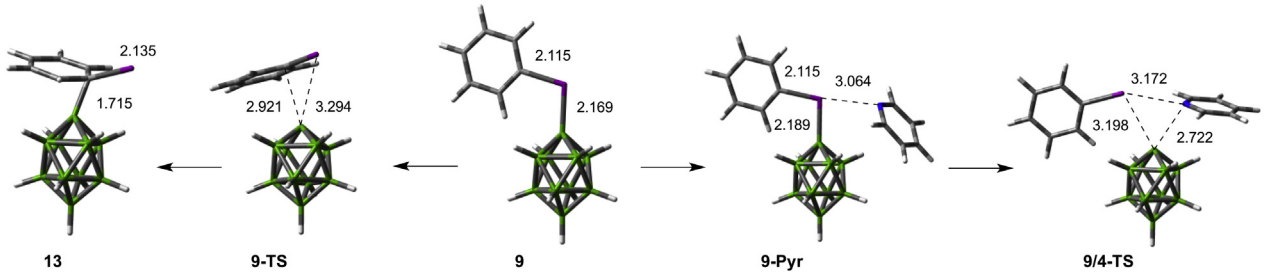

Fig. 12. Equilibrium geometry of species involved in transformations of [*closo*-$B_{10}H_9$-1-IPh]$^-$ (**9**, C_s molecular symmetry) at the M062x/6-31G(2d,p) level of theory. Selected interatomic distances are in Å.

activation for rearrangement of complex with Me_2NCHS, **1a-SDMF**, is higher by 0.6 kcal mol^{-1} than the rearrangement of free **1a** to **10** through the transition state **1a-TS** in Me_2NCHS dielectric medium. This result is consistent with low yields of isolated **2**. Noteworthy, complex of **1a** with Me_2NCHS (**1a-SDMF**) is much weaker than that with pyridine (**1a-Pyr**) due to the difference in the nucleophilicity of the S and N atoms.

Thus, computational results are consistent with experiments and demonstrate that aryliodonium zwitterions derived from [*closo*-$B_{12}H_{12}$]$^{2-}$ exhibit low stability against rearrangements, and low selectivity of product formation, when compared to the 10-vertex analogs. In general, aryliodonium zwitterions of [*closo*-$B_{12}H_{12}$]$^{2-}$ are the least stable among similar derivatives of [*closo*-1-$CB_{11}H_{12}$]$^-$, [*closo*-1-CB_9H_{10}]$^-$, [*closo*-$B_{10}H_{10}$]$^{2-}$, and Co-dicarbolide [16].

3. Discussion and conclusions

Detailed investigation of reactions of $ArI(OAc)_2$ with [*closo*-$B_{12}H_{12}$]$^{2-}$ led to the development of an efficient and convenient method for the preparation of mono-aryliodonium zwitterions [*closo*-$B_{12}H_{11}$-1-IAr]$^-$ **1**. Results demonstrate that the formation of **1** is a facile and fast process which occurs in aqueous acetic acid. The bis-zwitterions [*closo*-$B_{12}H_{10}$-$(IAr)_2$] were not observed in this reaction, and it appears that their formation requires more strongly acidic medium, such as 70% CF_3COOH [16]. Interestingly, the mono-aryliodonium zwitterions **1** are significantly less stable than the bis-zwitterions which can be purified by chromatography [16]. This is presumably related to the difference in electron density at the B—I bond in the mono- and bis-zwitterions. Salts of **1** are stable in the solid state, but decompose in CD_3CN solutions with first order kinetics consistent with a rearrangement of the free aryliodonium zwitterion (e.g. through **1a-TS**) or its complex with the solvent (the 10-I-3 species). Experimental and computational results agree that the 4-methoxyphenyliodonium derivative **1b** is more stable than the phenyliodonium **1a**. The former also gives higher yields of the substitution products.

Synthetic utility of the aryliodonium zwitterions **1a** and **1b** was demonstrated by the preparation of protected mercaptan **2** and by access to pyridinium derivative **3**. The synthesis is complicated and yields are diminished, however, by rearrangement of **1** and formation of {*closo*-B_{12}} arylation by-products, such as **5**. This undesired process is more pronounced for reactions with thioformamide than with pyridine, as evident from isolated yields and consistent with DFT calculations, and related to the ability of the reagent to coordinate the iodonium center in **1**. Despite low yields of the masked mercaptan **2** (25–27%), the presently described process is straightforward and convenient, when compared with those reported for [*closo*-$B_{12}H_{11}$-1-SH]$^{2-}$ obtained using different routes [13,22]. The present aryliodonium zwitterion method opens also a convenient access to pyridinium derivatives of [*closo*-$B_{12}H_{12}$]$^{2-}$; only two such derivatives have been prepared previously in a high

Please cite this article in press as: P. Tokarz, et al., Journal of Organometallic Chemistry (2015), http://dx.doi.org/10.1016/j.jorganchem.2015.07.035

temperature and low yield process [23,24].

Investigation of the solid-state structure for the [*closo*-$B_{10}H_9$-1-NC_5H_5]$^-$ (**4[NEt$_4$]**) and combustion analysis demonstrated the presence of the chlorine-substituted impurity in the crystal structure. Analysis of the route to **4[NEt$_4$]** revealed that [NEt_4]$^+$Cl$^-$ was used in phenyliodoniation of [*closo*-$B_{10}H_{10}$]$^{2-}$, and the Cl-anion was presumably oxidized with PhI(OAc)$_2$ to form electrophilic chlorine species. This process is even more pronounced with Br$^-$; no iodonium zwitterion **9** was obtained when [NEt_4]$^+$Br$^-$ was present in the reaction mixture [16]. These results suggest, however, a possible alternative method for the preparation of the 2-bromo and 2-iodo derivatives of the [*closo*-$B_{10}H_{10}$]$^{2-}$ anion.

A comparison of the electronic structures and spectral properties of **3** and **4** demonstrated a greater degree of electronic communication between the {*closo*-B_{10}} cluster and pyridine substituent than observed between {*closo*-B_{12}} and pyridine. These results are consistent with a general trend observed for other pairs of 10-vertex and 12-vertes derivatives [25,26].

Finally, extensive mechanistic analysis of transformations of aryliodonium zwitterions with the M06-2x method revealed a surprisingly good agreement between theory and experiment, despite the typically lower precision of such theoretical models and complex conformational potential energy surface of some of the involved species. Results allow for a detailed insight into the reaction mechanism and provide a convenient theoretical tool for analysis and understanding of other such reaction. For instance, computational analysis indicate that the boronium ylide **12** is more electrophilic than the 12-vertex analog **10**, as evident from the interactions with iodoarenes: while the 10-vertex intermediate **13** has a covalent character typical for products of electrophilic attack on the benzene ring, the 12-vertex ylide **10** appears to form much weaker sigma–pi complexes with the electron rich carbon atom in **11**.

The scope of substitution products derived from **1** is unclear at the moment and further investigation of reactions of **1** with other nucleophiles, such as AcO$^-$ and CN$^-$, is needed for its full evaluation as an intermediate to mono-substituted derivatives of the [*closo*-$B_{12}H_{12}$]$^{2-}$ cluster. Findings reported here impact the development and understanding of the fundamental chemistry of the [*closo*-$B_{12}H_{12}$]$^{2-}$ anion and contribute to our ongoing program in studying of liquid crystalline materials incorporating boron clusters [27].

4. Computational details

Quantum-mechanical calculations were carried out using the Gaussian 09 suite of programs [28]. Geometry optimizations were undertaken at either the B3LYP/6-31G(2d,p) (for TD-DFT calculations) or M062x/6-31G(2d,p) (for mechanistic studies) level of theory using tight convergence limits and appropriate symmetry constraints. Transition state structures were located using the QST3 method and input structures obtained from relaxed scans of the PES. Vibrational frequencies were used to characterize the nature of the stationary points and to obtain thermodynamic parameters. Zero-point energy (ZPE) corrections were scaled by 0.9806 [29]. Electronic excitation energies for **3** and **4** in MeCN dielectric medium were obtained at the B3LYP/6-31G(2d,p)//B3LYP/6-31G(2d,p) level using the time-dependent DFT method [30] supplied in the Gaussian package. Energy change in reactions were obtained at the M062x/6-31+G(2d,p)//M062x/6-31G(2d,p) level of theory in appropriate solvent dielectric medium implemented using the PCM model [31]. Calculations in pyridine medium were requested with the SCRF(solvent = Pyridine) keyword, while those in Me_2NCHS medium with SCRF(Solvent = Generic, Read) keyword and parameters “eps = 47.5” and “epsinf = 2.4775”. The NBO Population analysis of the DFT wavefunction was performed using the DENSITY(current) keyword.

5. Experimental section

5.1. General

Reagents and solvents were obtained commercially. Reactions and subsequent manipulations were conducted in air. NMR spectra were obtained at 128 MHz (^{11}B) and 400 MHz (^{1}H) in CD_3CN. ^{1}H NMR spectra were referenced to the solvent and ^{11}B NMR chemical shifts to an external sample of $BF_3\cdot Et_2O$ in CD_3CN (0 ppm). The preparation of 4-$MeOC_6H_4I(AcO)_2$ was described recently [16].

5.2. X-ray data collection

Single-crystal X-ray measurements for **3[NHEt$_3$]** and **4[NEt$_4$]** were performed with a Supernova Dual diffractometer equipped with an Atlas detector whereas for **3[NEt$_4$]** it was performed with a SuperNova diffractometer equipped with an Eos detector. All measurements were conducted at 100 K using the MoK_α radiation. The crystals were positioned at 74 and 50 mm from the Atlas and Eos detector, respectively. A total number of 570 and 709 frames were collected at 1° intervals with a counting time of 120s and 70s for **4[NEt$_4$]** and **3[NHEt$_3$]**, respectively. 499 frames were collected for **3[NEt$_4$]** with a counting time of 100s. The data were corrected for Lorentzian and polarization effects. Data reduction and analysis were carried out with the Crysalis program [32]. All structures were solved by direct methods and refined using SHELXL-97 [33] within the Olex2 program [34]. The refinement was based on F^2 for all reflections except those with very negative F^2. Weighted R factors (wR) and all goodness-of-fit (GooF) values are based on F^2. Conventional R factors are based on F with F set to zero for negative F^2. The $F_o^2 > 2\sigma(Fo^2)$ criterion was used only for calculating the R factors and it is not relevant to the choice of reflections for the refinement. The R factors based on F^2 are about twice as large as those based on F. Scattering factors were taken from the International Tables for Crystallography [35]. All hydrogen atoms were placed in idealized positions. In the case of **4[NEt$_4$]** modeling of the counterion disorder and the substitution of one of the hydrogen atoms of the boron cage by a chlorine atom was attempted. The final model resulted in two positions of the counterion with occupancy ratio of 20:80. Similarly, approximately 10% of {*closo*-B_{10}} molecules in the asymmetric part of the unit cell were modeled as substituted by chlorine atom in [*closo*-$B_{10}H_8$-6-Cl-1-NC_5H_5]$^-$.

The structures have been deposited at CCDC (1061528, 1061529, 1061530).

5.3. Preparation of [closo-$B_{12}H_{11}$-1-IAr]$^-$ [NEt_4]$^+$ (**1[NEt$_4$]**) and [closo-$B_{12}H_{11}$-1-IAr]$^-$ [$NHEt_3$]$^+$ (**1[NHEt$_3$]**). A general procedure

Aryliodonium diacetate [16] (11.0 mmol) was dissolved in glacial acetic acid (112 mL) and water (50 mL) was added. The solution was cooled in an ice bath and a solution of [NEt_4]$^+$OH$^-$ in water (35%, 4.5 mL, 11.0 mmol, for preparation of **1[NEt$_4$]**) or NEt_3 (1.5 mL, 11 mmol, for preparation of **1[NHEt$_3$]**) was added. Subsequently, a solution of sodium salt [*closo*-$B_{12}H_{12}$]$^{2-}$ 2Na$^+$ (1.88 g, 10.0 mmol) in acetic acid (25 mL) was added and the reaction mixture was vigorously stirred (mechanical stirrer). A white precipitate was formed immediately. The suspension was stirred for 30 min at ice bath temperature. Water (200 mL) was added and after 10 min of stirring, white solid was collected by filtration, washed with water and hexane and dried in air giving essentially pure monoiodonium product **1**, which was used without further purification.

Please cite this article in press as: P. Tokarz, et al., Journal of Organometallic Chemistry (2015), http://dx.doi.org/10.1016/j.jorganchem.2015.07.035

*5.3.1. [closo-$B_{12}H_{11}$-1-IPh]$^-$ [NEt_4]$^+$ (**1a[NEt_4]**)*

Yield 88%; ^{1}H NMR (300 MHz, CD_3CN, −20 °C) δ 0.2–2.3 (br m, 11H), 1.15 (tt, J_1 = 7.2 Hz, J_2 = 1.8 Hz, 12H), 3.10 (q, J = 7.3 Hz, 8H), 7.37 (t, J = 7.8 Hz, 2H), 7.58 (t, J = 7.4 Hz, 1H), 7.79 (d, J = 9.2 Hz, 2H); ^{13}C NMR (76 MHz, CD_3CN, −20 °C) δ 7.4, 52.4 (t, J = 3.0 Hz), 131.6, 131.9, 137.1; {^{1}H} ^{11}B (96 MHz, CD_3CN, −20 °C) δ −14.9 (6B), −14.3 (6B).

*5.3.2. [closo-$B_{12}H_{11}$-1-(IC_6H_4OMe-4)]$^-$ [NEt_4]$^+$ (**1b[NEt_4]**)*

Yield 95%; ^{1}H NMR (300 MHz, CD_3CN, −20 °C) δ 0.2–2.3 (br m, 11H), 1.16 (tt, J_1 = 7.3 Hz, J_2 = 1.7 Hz, 12H), 3.11 (q, J = 7.3 Hz, 8H), 3.79 (s, 3H), 6.91 (d, J = 9.1 Hz, 2H), 7.66 (d, J = 9.1 Hz, 2H); ^{13}C NMR (76 MHz, CD_3CN, −20 °C) δ 7.4, 52.5 (t, J = 3.0 Hz), 56.0, 92.5, 117.5, 138.4, 162.2; {^{1}H} ^{11}B (96 MHz, CD_3CN, −20 °C) δ −15.1 (6B), −14.2 (6B).

*5.3.3. [closo-$B_{12}H_{11}$-1-(IC_6H_4OMe-4)]$^-$ [$NHEt_3$]$^+$ (**1b[$NHEt_3$]**)*

Yield 74%; ^{1}H NMR (300 MHz, CD_3CN, −20 °C) δ 0.2–2.3 (br m, 11H), 1.19 (t, J = 7.3 Hz, 9H), 3.10 (qd, J_1 = 7.3 Hz, J_2 = 5.1 Hz, 6H), 3.79 (s, 3H), 6.55 (br t, J = 52 Hz, 1H), 6.91 (d, J = 9.0 Hz, 2H), 7.66 (d, J = 9.0 Hz, 2H); ^{13}C NMR (76 MHz, CD_3CN, −20 °C) δ 8.9, 47.4, 56.0, 92.5, 117.5, 138.5, 162.3; {^{1}H} ^{11}B (96 MHz, CD_3CN, −20 °C) δ −14.9 (6B), −14.2 (6B).

*5.4. Preparation of [closo-$B_{12}H_{11}$-1-$SCHNMe_2$]$^-$ [NEt_4]$^+$ (**2[NEt_4]**)*

N,*N*-Dimethylthioformamide (10 mL) was cooled to −10 °C in an ice-salt bath and 4-methoxyphenyliodonium derivative **1b[NEt_4]** (2.56 g, 5.0 mmol) was added in portions over 15 min. The mixture was stirred at −5 ÷ −10 °C overnight. All volatiles were removed under vacuum (0.1 mm Hg) and the viscous oily residue was treated with CH_2Cl_2 (3 mL). After two hours of stirring the resulting precipitate was collected by filtration and washed with CH_2Cl_2 giving 350 mg of off-white solid. The filtrate was evaporated under reduced pressure and treated again with a small portion of CH_2Cl_2, stirred for two hours, filtrated and the resulting solid was washed with CH_2Cl_2 giving 130 mg of off-white solid. The solids were combined giving 480 mg (27% yield) of the protected mercaptan **2[NEt_4]**, which was used for further transformations without additional purifications. An analytical sample was obtained by purification using preparative thin layer chromatography (CH_2Cl_2/MeCN, 10:3): mp 372 °C (decomp.); ^{1}H NMR (500 MHz, CD_3CN) δ 0.5–1.8 (br m, 11H), 1.18 (t, J = 7.3 Hz, 12H), 3.13 (q, J = 7.3 Hz, 8H), 3.19 (s, 3H), 3.39 (s, 3H), 9.18 (s, 1H); ^{13}C NMR (126 MHz, CD_3CN) δ 7.7, 41.7, 48.8, 53.0, 187.0; ^{11}B (160 MHz, CD_3CN) δ −15.2 (d, 1H), −14.0 (d, J = 129 Hz, 10B), −8.9 (s, 1B). Anal. Calcd. for $C_{11}H_{38}B_{12}N_2S$: C, 36.68; H, 10.63; N, 7.78. Anal. Calcd. for $C_{11}H_{38}B_{12}N_2S\cdot 1/2CH_2Cl_2$: C, 34.30; H, 9.76; N, 6.96. Found: C, 33.60; H, 10.07; N, 6.98.

*5.5. Preparation of [closo-$B_{12}H_{11}$-1-NC_5H_5]$^-$ [NEt_4]$^+$ (**3[NEt_4]**)*

Dry pyridine (15 mL) was cooled to −10 °C in an ice-salt bath, and 4-methoxyphenyliodonium derivative **1b[NEt_4]** (2.56 g, 5.0 mmol) was added in portions over 15 min. The mixture was stirred at −10 ÷ −5 °C overnight. All volatiles were removed under reduced pressure (0.1 mm Hg), the oily viscous residue was dissolved in MeCN and evaporated with a small portion of SiO_2. The resulting silica gel was loaded onto a SiO_2 column, washed with CH_2Cl_2 and then the product was eluted with a CH_2Cl_2/MeOH mixture (50:3). The crude product was crystallized from MeOH giving 764 mg (44% yield) of **3[NEt_4]** as colorless needles: mp 190–192 °C; ^{1}H NMR (500 MHz, CD_3CN) δ 0.5–2.0 (br, m, 11H), 1.19 (br t, J = 7.2 Hz, 12H), 3.13 (q, J = 7.3 Hz, 8H), 7.63 (t, J = 7.0 Hz, 2H), 8.15 (t, J = 7.7 Hz, 1H), 9.02 (d, J = 5.8 Hz, 2H); ^{13}C NMR (126 MHz, CD_3CN) δ 7.7, 53.1 (t, J = 2.3 Hz), 126.8, 143.3, 147.4; ^{11}B (160 MHz, CD_3CN) δ −16.6 (d, J = 126 Hz, 1B), −14.5 (d, J = 130 Hz, 10B), 0.0 (s, 1B). Anal. Calcd. for $C_{13}H_{36}B_{12}N_2$: C, 44.59; H, 10.36; N, 8.00. Found: C, 44.85; H, 10.55; N, 7.97.

A similar procedure using the phenyliodonium derivative **1a[NEt_4]** gave pyridinium **3[NEt_4]** in 12% yield. In addition, during chromatographic separation a second more polar oily fraction was isolated consisting of insertion product of [*closo*-$B_{12}H_{11}$-1-(C_6H_4I)]$^{2-}$: HRMS, calcd for $[B_{12}H_{15}C_6I]^{2-}$ m/z = 173.0673, found m/z = 173.0701.

*5.6. Preparation of [closo-$B_{12}H_{11}$-1-NC_5H_5]$^-$ [$NHEt_3$]$^+$ (**3[$NHEt_3$]**)*

The salt was obtained in 41% yield from **1b[$NHEt_3$]** according to the procedure for the preparation of **3[NEt_4]**: mp 198–200 °C; ^{1}H NMR (500 MHz, CD_3CN) δ 0.6–2.0 (br, m, 11H), 1.23 (t, J = 7.3 Hz, 9H), 3.14 (qd, J_1 = 7.3 Hz, J_2 = 5.1 Hz, 6H), 6.50 (br t, J = 53 Hz, 1H), 7.65 (t, J = 6.8 Hz, 2H), 8.17 (tt, J_1 = 7.6 Hz, J_2 = 1.4 Hz, 1H), 9.01 (d, J = 5.6 Hz, 2H); ^{13}C NMR (126 MHz, CD_3CN) δ 9.2, 48.1, 126.8, 143.3, 147.4. Anal. calcd. for $C_{11}H_{32}B_{12}N_2$: C, 41.02; H, 10.01; N, 8.70. Found: C, 41.30; H, 10.13; N, 8.54.

*5.7. Preparation of [closo-$B_{12}H_{11}$-1-$S(CH_2)_5$]$^-$ [NEt_4]$^+$ (**8[NEt_4]**)*

[*closo*-$B_{12}H_{12}$-$SCHNMe_2$][NEt_4] (**2[NEt_4]**, 270 mg, 0.75 mmol) was dissolved in MeCN (10 mL), [NEt_4]$^+$OH$^-$ (35% in water, 947 mg, 2.25 mmol) was added, followed by a solution of 1,5-dibromopentane (173 mg, 0.75 mmol) in acetonitrile (10 mL). The solution was gently refluxed overnight and evaporated to dryness in *vacuo*. The residue was suspended in water. The resulting white solid was collected by filtration and washed several times with water and hexane, giving 280 mg of crude product. The product was further crystallized from MeOH giving 230 mg (82% yield) of sulfonium **8[NEt_4]** as white crystals: mp 238–240 °C; ^{1}H NMR (500 MHz, CD_3CN) δ 0.6–1.8 (br, m, 11H), 1.97 (tt, J_1 = 7.3 Hz, J_2 = 2.8 Hz, 12H), 1.39 (qt, J_1 = 12.8 Hz, J_2 = 3.6 Hz, 2H), 1.62–1.78 (m, 2H), 2.09 (dm, J = 15.3 Hz, 2H), 2.79 (td, J_1 = 13.0 Hz, J_2 = 2.4 Hz, 2H), 3.01 (br d, J = 13.9 Hz, 2H), 3.15 (q, J = 7.2 Hz, 8H); ^{13}C NMR (126 MHz, CD_3CN) δ 7.7, 24.8, 25.0, 39.1, 53.0 (t, J = 11 Hz); ^{11}B (160 MHz, CD_3CN) δ −15.5 (d, J = 126 Hz, 5B), −13.9 (d, J = 132 Hz, 5B), −13.30 (d, 1B), −10.1 (s, 1B). Anal. Calcd. for $C_{13}H_{36}B_{12}N_2$: C, 41.83; H, 11.07; N, 3.75. Found: C, 41.91; H, 11.08; N, 3.75.

5.8. Kinetic measurements

The decomposition of iodonium zwitterions **1[NEt_4]** in CD_3CN at 0 °C was monitored by ^{1}H NMR. The solvent was cooled to about −25 °C, small amount of dimethyl terephthalate as the reference was added followed by about 3 mg of the zwitterion. The spectrometer was thermostated prior to introduction of the NMR tube. The ratio of the intensity of the most downfield (7.80 ppm, for **1a[NEt_4]**) or upfield (7.66 ppm, **1b[NEt_4]**) signals of the aromatic protons and reference (8.06 ppm) was calculated. A plot of log of the ratio *vrs* time (30 min for **1a[NEt_4]**, and 50 min for **1b[NEt_4]**) gave the decomposition rate.

The major organic product of decomposition of [*closo*-$B_{12}H_{11}$-1-IPh]$^-$ [NEt_4]$^+$ (**1a[NEt_4]**) was identified as iodobenzene: ^{1}H NMR (500 MHz, CD_3CN) δ 7.15 (t, J = 7.7 Hz, 2H), 7.38 (tt, J_1 = 7.5 Hz, J_2 = 1.1 Hz, 1H), 7.73 (dd, J_1 = 8.6 Hz, J_2 = 1.1 Hz, 2H). Other signals include δ 6.90–7.01 (m), 7.28–7.32 (m), 7.45–7.60 (br m).

The major organic product of decomposition of [*closo*-$B_{12}H_{11}$-1-(IC_6H_4OMe-4)]$^-$ [NEt_4]$^+$ (**1b[NEt_4]**) was identified as 4-iodoanisole: ^{1}H NMR (300 MHz, CD_3CN) δ 3.75 (s, 3H), 6.74 (d, J = 8.9 Hz, 2H), 7.59 (d, J = 8.9 Hz, 2H). Other signals include δ 3.72 (s), 6.50 (br d), 6.61 (d), 6.92 (t), 7.16 (br d), 7.44 (br m).

The zwitterion **6** was identified by MS in both samples: HRMS, calcd for $[B_{12}H_{11}C_2D_3N]^-$ m/z = 186.2473, found m/z = 186.2489.

Please cite this article in press as: P. Tokarz, et al., Journal of Organometallic Chemistry (2015), http://dx.doi.org/10.1016/j.jorganchem.2015.07.035

Acknowledgments

This work was supported by the NSF grant (DMR-1207585). We thank Dr. Jacek Pecyna for technical assistance.

Appendix A. Supplementary data

Supplementary data related to this article can be found at http://dx.doi.org/10.1016/j.jorganchem.2015.07.035.

References

[1] I.B. Sivaev, V.I. Bregadze, S. Sjöberg, Collect. Czech. Chem. Commun. 67 (2002) 679.
[2] A.H. Soloway, W. Tjarks, B.A. Barnum, F.-G. Rong, R.F. Barth, I.M. Codogni, J.G. Wilson, Chem. Rev. 98 (1998) 1515.
[3] I.B. Sivaev, V.V. Bregadze, Eur. J. Inorg. Chem. (2009) 1433.
[4] I.B. Sivaev, V.I. Bregadze, N.T. Kuznetsov, Russ. Chem. Bull. 51 (2002) 1362.
[5] D. Olid, R. Núñez, C. Viñas, F. Teixidor, Chem. Soc. Rev. 42 (2013) 3318.
[6] I.B. Sivaev, V.I. Bregadze, S. Sjöberg, Russ. Chem. Bull. 47 (1998) 193.
[7] F. Alam, A.H. Soloway, R.F. Barth, N. Mafune, D.M. Adams, W.H. Knoth, J. Med. Chem. 32 (1989) 2326.
[8] A.A. Semioshkin, I.B. Sivaev, V.I. Bregadze, Dalton Trans. (2008) 977.
[9] W.H. Knoth, H.C. Miller, J.C. Sauer, J.H. Balthis, Y.T. Chia, E.L. Muetterties, Inorg. Chem. 3 (1964) 159.
[10] O. Haeckel, W. Preetz, Z. Anorg. Allg. Chem. 621 (1995) 1454.
[11] L.I. Zakharkin, G.L. Zhigareva, Russ. J. Gen. Chem. 71 (2001) 83.
[12] T. Peymann, C.B. Knobler, M.F. Hawthorne, Inorg. Chem. 37 (1988) 1544.
[13] E.I. Tolpin, G.R. Wellum, S.A. Barley, Inorg. Chem. 17 (1978) 2867.
[14] A.A. Semioshkin, P.V. Petrovskii, I.B. Sivaev, E.G. Balandina, V.I. Bregadze, Russ. Chem. Bull. 45 (1996) 683.
[15] W.R. Hertler, M.S. Raasch, J. Am. Chem. Soc. 86 (1964) 3661.
[16] P. Kaszyński, B. Ringstrand, Angew. Chem. Int. Ed. 54 (2015) 6576.
[17] J. Poater, M. Sola, C. Vinas, F. Teixidor, Angev. Chem. Int. Ed. 53 (2014) 12191.
[18] For more details see the ESI.
[19] B. Ringstrand, P. Kaszyński, V.G. Young Jr., Z. Janoušek, Inorg. Chem. 49 (2010) 1166.
[20] J. Pecyna, B. Ringstrand, S. Domagała, P. Kaszyński, K. Woźniak, Inorg. Chem. 53 (2014) 12617.
[21] P. Kaszyński, S. Ciastek, P. Tokarz, V.G. Jr. Young. Unpublished results.
[22] W.H. Knoth, J.C. Sauer, D.C. England, W.R. Hertler, E.L. Muetterties, J. Am. Chem. Soc. 86 (1964) 3973.
[23] T. Koch, W. Preetz, Z. Naturforsch. B 52 (1997) 1165.
[24] A. Vöge, E. Lork, B.S. Sesalan, D. Gabel, J. Organometal. Chem. 694 (2009) 1698.
[25] P. Kaszyński, S. Pakhomov, V.G. Young Jr., Collect. Czech. Chem. Commun. 67 (2002) 1061.
[26] S. Pakhomov, P. Kaszyński, V.G. Young Jr., Inorg. Chem. 39 (2000) 2243.
[27] P. Kaszyński, in: N. Hosmane (Ed.), Boron Science: New Technologies & Applications, CRC Press, 2012, p. 305.
[28] M.J. Frisch, G.W. Trucks, H.B. Schlegel, G.E. Scuseria, M.A. Robb, et al., Gaussian 09, Revision A.02, Gaussian, Inc., Wallingford CT, 2009.
[29] A.P. Scott, L. Radom, J. Phys. Chem. 100 (1996) 16502.
[30] R.E. Stratmann, G.E. Scuseria, M.J. Frisch, J. Chem. Phys. 109 (1998) 8218.
[31] M. Cossi, G. Scalmani, N. Rega, V. Barone, J. Chem. Phys. 117 (2002) 43.
[32] Agilent, CrysAlis PRO, Agilent Technologies, Yarnton, England, 2012.
[33] G.M. Sheldrick, Acta Crystallogr. A 64 (2008) 112.
[34] O.V. Dolomanov, L.J. Bourhis, R.J. Gildea, J.A.K. Howard, H. Puschmann, J. Appl. Crystallogr. 42 (2009) 339.
[35] U. Schmueli (Ed.), International Tables for Crystallography, Springer, New York, 2006.